ENHANCED IMAGING OF CORROSION IN AIRCRAFT STRUCTURES WITH REVERSE GEOMETRY X-RAY ®

William P. Winfree [a], Noreen A. Cmar-Mascis [b], F. Raymond Parker [a]

[a] NASA Langley Research Center, MS 231, Hampton VA 23681-2199

[a] U.S. Army Research Laboratory - Vehicle Technology Center, NASA Langley ResearchCenter,MS231,HamptonVA23681-2199

Abstract

The application of Reverse Geometry X-ray ® to the detection and characterization of corrosion in aircraft structures is presented. Reverse Geometry X-ray® is a unique system that utilizes an electronically scanned x-ray source and a discrete detector for real time radiographic imaging of a structure. The scanned source system has several advantages when compared to conventional radiography. First, the discrete x-ray detector can be miniaturized and easily positioned inside a complex structure (such as an aircraft wing) enabling images of each surface of the structure to be obtained separately. Second, using a measurement configuration with multiple detectors enables the simultaneous acquisition of data from several different perspectives without moving the structure or the measurement system. This provides a means for locating the position of flaws and enhances separation of features at the surface from features inside the structure. Data is presented on aircraft specimens with corrosion in the lap joint. Advanced laminographic imaging techniques utilizing data from multiple detectors are demonstrated to be capable of separating surface features from corrosion in the lap joint and locating the corrosion in multilayer structures. Results of this technique are compared to computed tomography cross sections obtained from a microfocus x-ray tomography system. A method is presented for calibration of the detectors of the Reverse Geometry X-ray ® system to enable quantification of the corrosion to within 2%.

Keywords: x-ray, radiography, corrosion, aircraft, computed tomography, laminography, NDE

Introduction

The life of the aircraft can be considerably extended by early detection of corrosion and by taking corrective action to remove and arrest corrosion of the structure. As the age of an aircraft increases, the importance of detection of corrosion increases because there is an increased probability of an interaction between the corrosion and other forms of damage such as fatigue cracks. The detection of corrosion without disassembly of the aircraft prevents the possibility of aggravating the issue by removing effective sealant.

The most common technique for detecting corrosion in aircraft is visual inspection for surface distortions or pillowing of the outer skin. Advanced NDT techniques are employed when regions are partially or completely inaccessible for inspection due to the overlying structure. Most of these techniques have difficulty accurately quantifying the corrosion, particularly in complex or

multilayered structures.

The application of a recently developed radiographic technique known as Reverse Geometry X-ray® (RGX®)[1-4] to the detection of corrosion is described in this paper. Reverse Geometry X-ray® is a unique system for real time radiographic imaging of a structure. This system has several possible advantages compared to conventional radiography. First, the x-ray detector can be miniaturized and easily positioned inside a complex structure (such as an aircraft wing) enabling images of each surface of the structure to be obtained separately. Second, multiple detectors enable the simultaneous acquisition of data from several different perspectives without moving the structure or the measurement system. This provides a means for locating the position of flaws and enhances separation of features at the surface from features inside the structure. Finally, the amount of secondary scattered radiation contributing to the noise in the radiograph is reduced compared to conventional radiography. This simplifies the conversion of the radiographs to quantitative images of the integrated material density along the ray paths between the source and the detector.

Reverse Geometry X-ray System®

A simplified schematic of the Reverse Geometry X-ray® system is shown in figure 1. The most unique feature of the system is the large scanned x-ray source with a target diameter of approximately 25 cm. The x-ray source operates in a manner similar to a video monitor. An electron beam is electronically rastered over the inner surface of the front of the x-ray source. Where the electrons collide with the inner surface of the tube, x-rays are generated. By electronically scanning the electron beam, the instantaneous position of the x-ray source is scanned over an area of the front surface of the tube. The size and location of the scanned region is user definable and varies from the whole front surface to an area approximately 5 cm by 5 cm. The repetition rate of the scan is user definable, variable from 0.25 seconds to 16 seconds. The acceleration voltage is also user definable from 55 to 160 kV with an electron beam current up to approximately 0.5 mA. The diameter of the electron beam spot at the inner surface of the tube is approximately 25 microns.

The intensity of the x-ray flux is recorded with a relatively small NaI(Ti) scintillation detector coupled to a photomultiplier tube. The photomultiplier tube output is amplified and offset before being digitized by a data acquisition computer. This enables optimizing the dynamic range of the digitizer to the dynamic range of the acquired signal. A detector is placed 81 cm above the center of the tube. Seven other detectors are placed at positions circling the tube at distances varying from 29 to 38 cm from the center and at a height of 36 cm above the surface of the tube. The detectors enable the acquisition of three dimensional data about a specimen. The data acquisition computer is connected to all eight detectors through a multiplexer enabling electronic switching between detectors.

The specimen of interest is placed on top of the x-ray source. This is the opposite of conventional radiography where the object is placed near an imaging detector and the source is approximately a point source. The data acquisition computer also controls the rastering of the electron beam. By acquiring the output of the detector as a function of electron beam position, the computer is able to generate a real-time radiograph of the specimen of interest.

Figure 1. Schematic of Reverse Geometry X-ray® System.

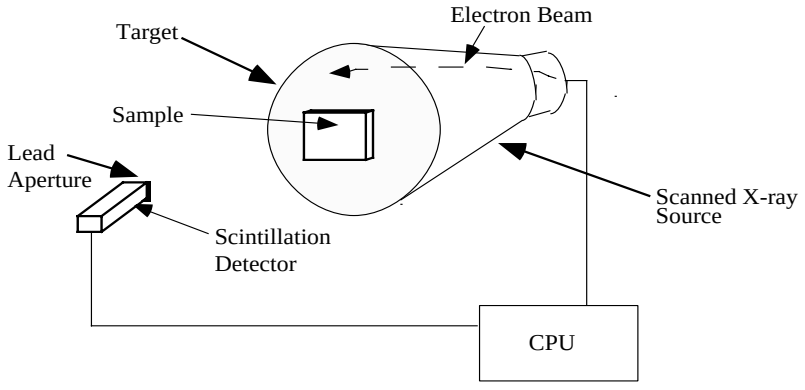

Computer Tomographic Inspection

For the corroded aircraft sections, computer tomographic (CT) images were collected using a third generation microfocus x-ray CT system. The microfocus x-ray source for the tomography system was operated at 160 KV with a spot size of 50 microns and a current of 0.3 mA. The scintillator based x-ray detector package consisted of 8192 photodiodes spaced on 25 microns centers. The photodiodes were cooled to -40^{o} C to minimize the effect of dark current.

The thickness of the CT slices was set to 0.3 - 1 mm by adjustment of tungsten collimators, which also reduced the amount of scatter reaching the detectors. Projection data were collected over one complete rotation at 1 degree increments integrating for 10 seconds at each projection. The projection data were corrected for the effects of dark current in the photodiodes and x-ray intensity variations. The corrected projection data were reconstructed using a fan beam back projection routine.

Reduction of Radiographs to Thickness Measurements

A simple analysis technique is desired for conversion of the radiographic data to material thickness. Previous efforts[5] have focused on using measurements both before and after placing a specimen in the field of view. Additionally, careful procedures were used to insure the signal levels for no specimen and no x-rays were known during the measurement process. For application in the field, it is desirable to use less complicated calibration procedures which rely on nominal thicknesses for the structure or the thickness of a thin shim placed in the field of view. This section discusses a simplified calibration procedure.

For a pencil beam geometry, the fluence of monochromatic photons in a homogeneous material is attenuated according to Beer's law [6]:

$$\Phi(x) = \Phi_0 e^{-\mu x} \tag{1}$$

where $\Phi(x)$ is the photon fluence after traveling x distance in the material, Φ_o is the photon fluence incident on the material and μ is the linear attenuation coefficient for the material. If the material is thin relative to the linear attenuation coefficient such that $\mu L << 1$, where L is the

distance traversed in the material, the fluence exiting the material simplifies to: (2)

$$\Phi(L) = (1-\mu L)\Phi_0 \quad , \tag{3}$$

or the change in fluence is proportional to the thickness of the material. For aluminum and x-ray energies on the order of 70 keV, this is a good approximation up to several mm of material. Since most aircraft fuselages are less than 3 mm in thickness, this is a reasonable approximation for fuselage inspections. (4)

The detector output is proportional to the fluence incident on the detector and is given by:

$$D(L) = (1-\mu L)Q\Phi_0 \quad , \tag{5}$$

where Q is a constant proportional to the size and efficiency of the detector. The detector output is amplified and offset before digitization, therefore the digitized signal is given by: (6)

$$S(L) = (1-\mu L)GQ\Phi_0 + O \quad , \tag{7}$$

where G is the gain of the amplifier and O is the offset. This can be rewritten as: (8)

$$S(L) = AL + B \quad , \tag{9}$$

where $A = -GQ\mu F_0$ and $B = O+GQF_0$. If the thickness at two points in the image is known, A and B can be solved for to convert the image into an image of the thickness of the material. If there exists a known change in thickness (such as from placing a shim in the image), then it is possible to determine A and generate an image of the change in thickness of the material. (10)

Equation (2) represents the first order expansion of the exponential equation in Beer's law yielding a linear relationship between the thickness and the signal level. The second order expansion of the exponential equation gives a similar expression for the signal:

$$S(L) = \left(1-\mu L+\frac{\mu^2 L^2}{2}\right)GQ\Phi_0 + O \quad . \tag{11}$$

This equation can be represented as three independent parameters in the form of a quadratic equation. Therefore the relationship between signal and thickness is given by:

$$S(L) = AL + B + CL^2 \quad , \tag{12}$$

where $C = GQ\mu^2\Phi_0/2$. By performing measurements at three different thicknesses, it is possible to calibrate the detector. (13)

Results of Measurement on Variable Thickness Sample

A sample was fabricated to test the quantitative capabilities of measuring the material thickness using the simplified calibration procedure. A ramped thickness sample was fabricated

Figure 2. Schematic of Al 2024 specimen with ramped thickness.

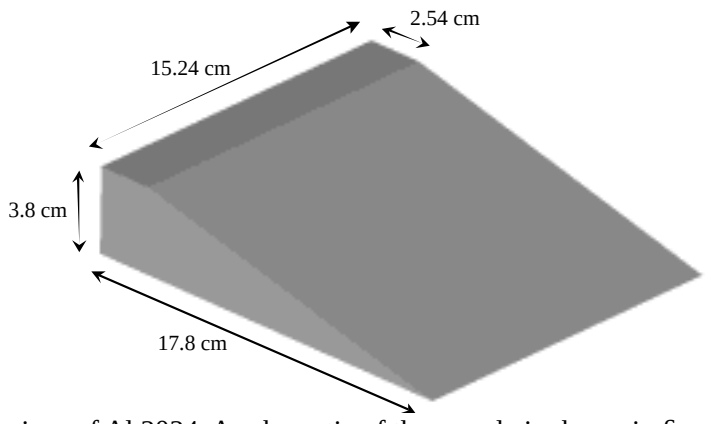

from a 3.8 cm thick piece of Al 2024. A schematic of the sample is shown in figure 2.

A radiograph of the sample is shown in figure 3. The radiograph is displayed with the thinnest region of the specimen on the left hand side of the image and the thickest region on the right hand side of the image. The image shows an increase in signal amplitude, represented by lighter shades, with increasing thickness.

The monotonic increase in signal with specimen thickness is illustrated in figure 4, which displays the calibrated data along a line through the vertical center of the specimen plotted against the thickness of the specimen. Values for A and B in equation (5) are determined by performing a linear fit of the data for the region of the sample where the thickness is less than 1 cm. The figure clearly displays the initial linear relationship between the thickness of the specimen and the calibrated thickness from the radiograph. Also shown on the plot is the difference in the

Figure 3. Radiographic image of aluminum sample with ramped thickness.

Figure 4. Comparison of mechanical measurement of thickness and estimation of thickness from radiographic measurements using calibration based on linear approximation. Also shown is the difference between the radiographic and mechanical measurements.

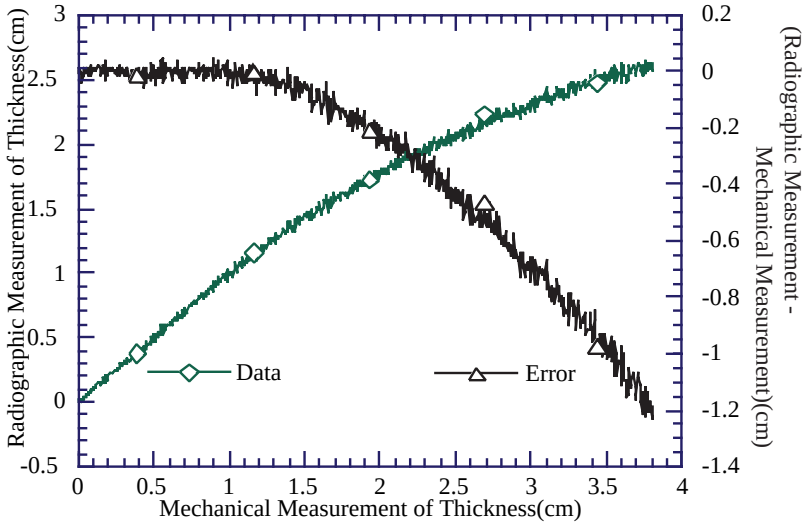

mechanical measurement and the radiographic measurement for thickness. The plots also indicate a calibration error which is much larger than the random error when the aluminum thickness is greater than 1 cm. For thicknesses less than 1 cm, the standard deviation in the signal is 0.01 cm. This value can be considerably reduced, if the measurement is performed over an area rather than at a single point. The calibration error becomes significant at thicknesses greater than 1 cm largely due to the approximation of equation 2 no longer being appropriate.

Using the second order approximation given in equation (7), the signal amplitude for all thicknesses was fitted using a quadratic equation. The quadratic equation was then inverted to give the calibration for thickness as a function of signal level. Figure 5 shows the results of this calibration for a line across the center of the sample. For this approximation, there is good agreement between the thickness as calculated from the radiographic and mechanical measurements. From the calibration coefficients, it is possible to calculate the effective linear attenuation coefficient for the aluminum sample ($\mu_{effective}$ =2*C/A). This yields a value for the effective linear attenuation coefficient of 0.522/cm, which corresponds to the linear attenuation coefficient of Al with a density of 2.7 gm/cm3 at 84 keV. This value for effective attenuation is reasonable, since 84 keV is near the peak of the measured spectrum of the x-ray tube for the operating acceleration voltage of 120KV.

Consideration of the error for this calibration technique indicates there is increasing calibration error for thicknesses greater than 1cm. This may be due in part to the Beer's law giving the attenuation for a monochromatic x-ray spectrum, while the measurement system has a polychromatic spectrum. The random noise also increases significantly for thicker regions of the sample due to photon counting statistics. The standard deviation in the thickness measurement for thicknesses less than 1 cm remains approximately 0.01 cm. This represents the accuracy of the measurement at a single point in the image. Since in practice the area of interest for the measurement is typically greater than the area of one pixel in the image, values can be averaged over an area of interest resulting in a measurement which is considerably more accurate that the

Figure 5. Comparison of mechanical and radiographic measurements of the thickness of different points on the wedge using calibration based on second order approximation and difference between radiographic and mechanical measurement.

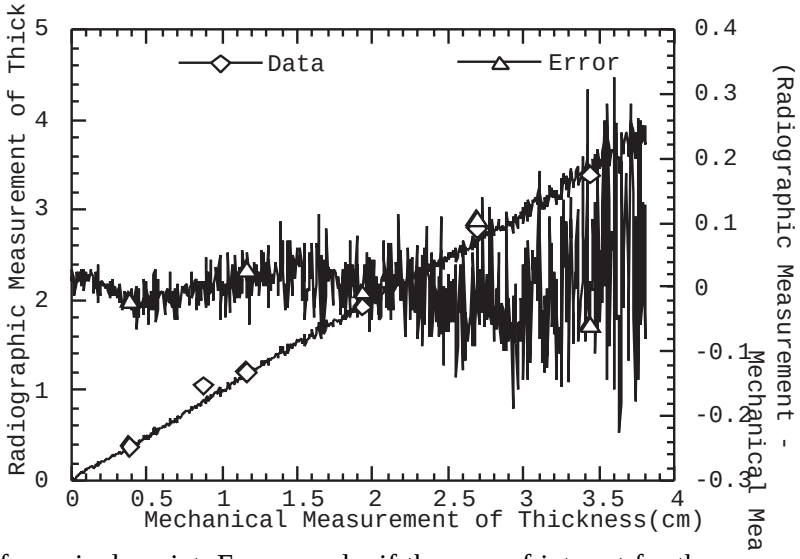

measurement for a single point. For example, if the area of interest for the measurement is 0.04 mm^2, measurement accuracies of 0.01 mm are possible.

Imaging Corrosion in Aircraft Specimen

Detection and quantification of corrosion in real aircraft specimens is considerably more

Figure 6. Radiographic image of aircraft specimen with significant corrosion. (a) Image scaled to display feature of specimen. (b)Image scaled to feature corroded region of specimen.(c) Histogram equalized image of the corroded region.

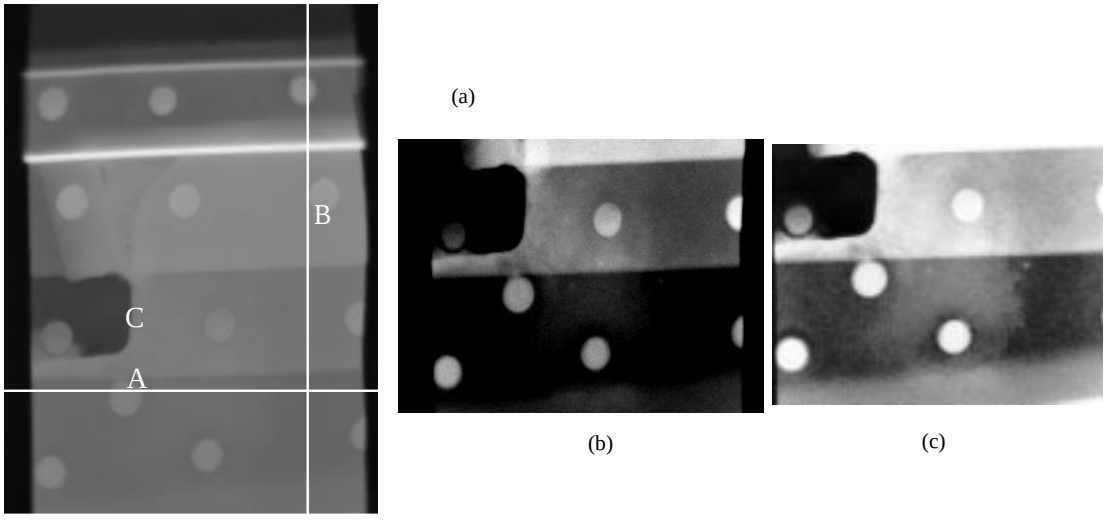

Figure 7. 3D rendering of corrosion region data from detector 8 of digiray system

difficult than quantifying variations in thickness in a fabricated specimen. The image of a typical lap joint specimen in figure 6a illustrates this difficulty. The specimen, obtained from an aircraft fuselage, has several different thicknesses. Linear scaling of the image contrast to enable the visualization of the variable thicknesses in the specimen, masks the slight variation resulting from the corrosion in the sample. Improved visualization of the corrosion is obtained by performing a linear stretch of the contrast as is shown in figure 6b, which scales the image to enable visualization of the corrosion for a single thickness of the specimen. An alternate technique which enables the rapid visualization of corrosion in a specimen with multiple thicknesses is histogram equalization. The region of the specimen displayed in figure 6b, is also displayed in figure 6c with the histogram equalized. This gives the best gray scale presentation of the corrosion. Since histogram equalization is a nonlinear process, the quantitative nature of the data is lost.

Examination of the images in figure 6 illustrates a difficulty in quantification of corrosion in real specimens. The corroded areas of the specimen have the appearance of having more material rather than less. This can be readily seen in an alternate representation of the data. Following calibration of the data, a three dimensional volume can be constructed by assuming a flat bottom for the sample and a voidless, homogeneous structure. The vertical voxels of the volume representation are filled with fixed values until the projection through the volume

Figure 8. Thickness profile of specimen at line C of figure 6.

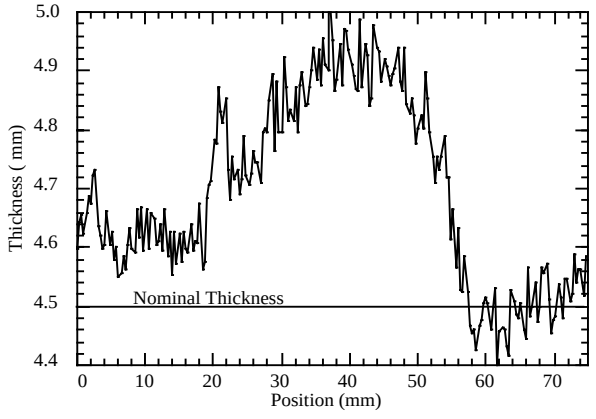

Figure 9. X-ray tomographic images of corroded aircraft specimen, (a) along line A of figure 6a, and (b) along line B of figure 6a.

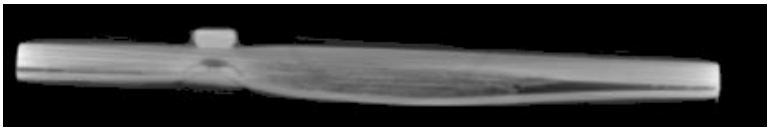

(a)

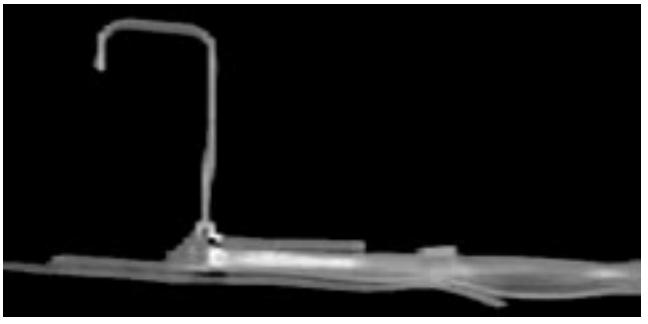

(b)

representation is equal to the measured projection through the specimen. This reconstructed volume is then displayed with a volume visualization algorithm. For the specimen in figure 6, the results of this procedure are shown in figure 7. The region of corrosion appears as an increase in the apparent thickness of the material.

The apparent increase in material thickness is a result of the radiographic intensities being a function of the total mass along the ray path between the source and the detector. As the material corrodes, the aluminum of the structure combines with other elements to produce corrosion by-products. These by-products are sometimes trapped within the structure. The net mass along the ray path is the mass of the residual material plus the mass of the by-products. This increase in net mass results in an increase rather than a decrease in the attenuation of the x-rays, which gives the appearance of an increase in material thickness rather than a decrease. This apparent increase in thickness is clearly seen in figure 8 which shows the profile of thickness along line C in figure 6a. Most of the profile indicates a thickness which is greater than the nominal thickness of the material.

The x-ray tomographic images in figure 9 help to provide insight into the nature of corrosion and the difficulty of quantifying it with radiographic techniques. X-ray tomography enables viewing cross sections of the material, without disturbing either the delicate structure of the residual material or the location of the by-products. Figures 9a and 9b are cross sections of the specimen along lines A and B in figure 6a. Both images show the distortion or pillowing of the surfaces due to the corrosion of the material. This distortion of the material also contributes to the apparent increase in thickness of the material. Figure 9a indicates a region of lower density under the rivet head resulting from either the formation of a pocket of corrosive by-products under the rivet head or an air pocket caused by the deformation of the structure. The nature of corrosion, as illustrated in these cross sections, makes it difficult to quantify with any technique. However, the increase in apparent thickness is a good indicator as to the presence of corrosion.

The detectability of the corrosion with radiography can be further improved with digital laminography. Laminography is performed by imaging the specimen from several different angles. These images are all back projected and summed to yield an image which highlights the

Figure 10. Laminographic images of the corroded aircraft specimen, with planes (a) at the interface between the top and bottom layers of the lap joint and (b) at the depth containing the formed heads of the rivets

(a) (b)

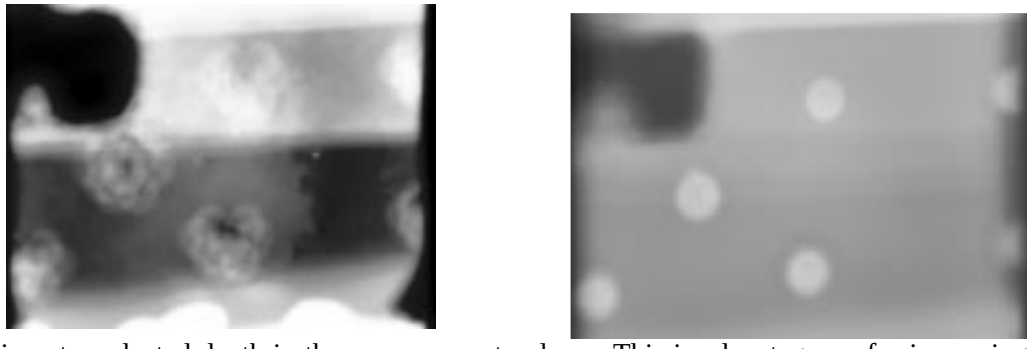

information at a selected depth in the measurement volume. This is advantageous for increasing the detectability of corrosion that exists at a known location, for example, at the interface between two layers. The Reverse Geometry X-ray® system is ideally suited to digital laminography as the source position is electronically scanned. Several detectors collect data at different locations around the specimen to provide the different angles required for laminography.

In figure 10, the data from eight detectors are reconstructed to highlight the information at the interface between the layers of the lap joint (figure 10a) and to highlight the information at the depth of the formed rivet heads of the lap joint (figure 10b). A comparison of figures 10a and 10b show the type of information obtainable from laminography. In figure 10b, the contributions from the formed rivet heads to each of the obtained radiographs are collocated in the reconstructed image. They reinforce each other, improving their contrast with respect to the rest of the image.

Figure 10a is the reconstructed image for the depth of the interface between two layers in the structure. Here the contributions from the corrosion from the different images reinforce each other to improve their contrast relative to the rest of the specimen. This image gives improved definition of the region of corrosion as compared to images in figures 6b and 6c. This image also verifies that the radiographic indications of corrosion, which appear in figures 6b and 6c, are from material in the plane between the layers of the lap joint. One limitation of this simple

Figure 11. (a)Radiograph of aircraft specimen obtained from detector directly above specimen and (b) same image following removal of formed rivet head contribution from image.

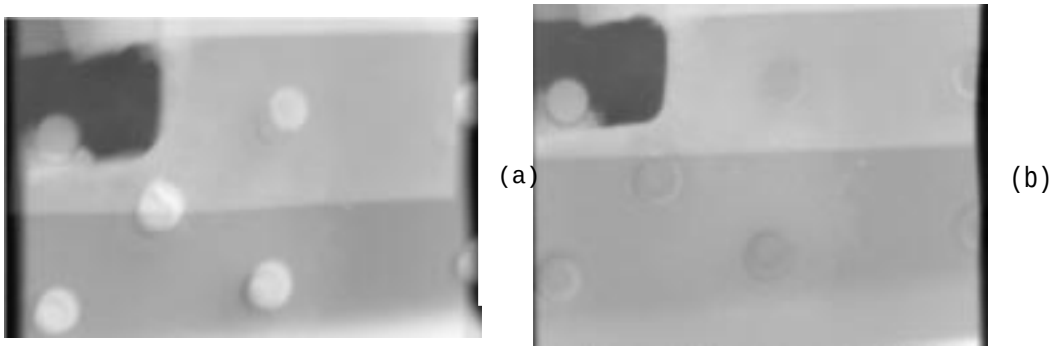

Figure 12. Laminographic images of the corroded aircraft specimen, with planes at the interface between the top and bottom layers of the lap joint obtained from data with formed rivet head contribution removed.

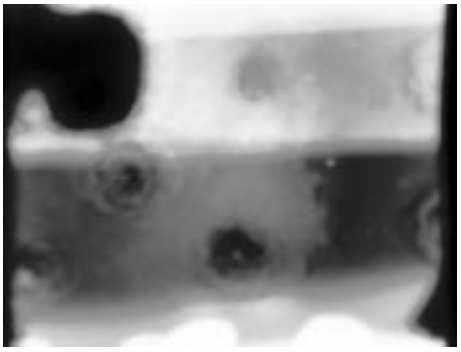

laminographic technique is that the contribution from the formed rivet heads is distributed around the region of the rivet and masks the information in that region.

The contribution from the formed rivet heads can be partially removed from the data by using the data from figure 10b. These data represent the combined contribution of the formed rivet heads from all of the eight radiographs.Using these data, an image can be constructed which contains only the contribution of the formed rivet heads. This data is projected back to the planes of the acquired data, then subtracted from the radiographs. The result is an image with a significant reduction in the contribution from the formed rivet heads. Figure 11 show the results of this process. Figure 11a is the as-received image from the detector directly above the specimen. Figure 11b shows the same data following the removal of the contribution from the formed rivet heads. This figure shows that the contribution from the formed rivet heads is significantly reduced.

Using the images with the contributions from the formed rivet heads removed, the laminographic reconstruction highlighting the data from the depth corresponding to the corrosion is shown in figure 12. In this image, the contribution from the formed rivet heads is significantly reduced, however not totally eliminated. In this image, it is possible to visualize the corrosion closer to the rivet. Future efforts will involve interative processing of the data to improve separation of information from different layers.

9. Summary

A method has been presented for reducing data from a Reverse Geometry X-ray® system to precise images of the material thickness by calibrating the data using known thicknesses within the images. Using a second order approximation of Beer's equation, good agreement was achieved between the radiographic and mechanical measurements of thickness.

The Reverse Geometry X-ray® system is also shown to be capable of imaging the effects of corrosion on a real aircraft specimen. Due to the nature of the corrosion, the radiograph gives the appearance of increased thickness in the corroded area. This makes quantification of the extent of corrosion difficult. Laminographic image reconstruction utilizing data from the eight detectors is presented. Laminographic reconstruction of planes of interest within the lap joint is demonstrated to increase the detectability of the corrosion effects. A method for removal of surface features from images of interior planes of interest is shown to improve corrosion boundary definition.

References

1.The phrase “Reverse Geometry X-ray”® and RGX® are registered trademarks of Digiray Corporation, San Ramon, CA.
2. U.S. Patent 3,949,229 (April 6,1976), R.D. Albert.
3. T.M. Albert, Review of Progress in Quantitative Nondestructive Evaluation, 13, 587(1994).
4. T.M. Albert, 1993 JANNAF Nondestructive Evaluation Subcommittee Meeting, The Johns Hopkins University/Chemical Propulsion Information Agency Publication 596, 1993, pp. 71-83.
5. E.A. Birt, F.R.Parker and W.P.Winfree, Review of Progress in Quantitative Nondestructive Evaluation, 13, 1963(1994).
6. H.H. Barrett and W. Swindell, Radiographic Imaging, The Theory of Image Formation, Detection, and Processing, Vol. 1, Academic Press, New York, 1981, pp 316
7. R. L. Webber, R.A. Horton, D.A. Tyndall, J.B. Ludlow, Dento Maxillo Facial Radiology, 26,(1),53,(1997)
8. U. Ewert, J. Robbel, C. Bellon, A. Schumm, C. Nockemann, MaterialPrufung, 37,(6),218,(1995)
9. A.R. Kalukin and V. Sankaran, IEEE Transactions on Components, Packaging and Manufacturing Technology-Part A, 20,(Y),1,(1997)